Earth, Planets and Space

FULL PAPER

Open Access

Physical mechanism for the temporary intensification of wintertime sporadic E layers in 2009

Satoshi Andoh[1*], Akinori Saito[2] and Hiroyuki Shinagawa[3]

Abstract

This study provides a physical mechanism for the temporary intensification of wintertime sporadic E layers (EsLs) in 2009. It is widely accepted that vertical wind shears control EsL formations. EsL intensity is minimal in winter, partially because of the weakened vertical wind shears. Despite the wintertime minimum EsL intensity, temporary intensifications of EsLs occurred for 10–30 days in some winters, the cause of which remains unclear. In this study, we conducted month-long EsL simulations in 2009 and 2011, the years when both wintertime EsL (WiEsL) intensification and sudden stratospheric warming (SSW) occurred, and when neither did, respectively. The simulations aimed to reveal the physical mechanisms of the WiEsL intensification in 2009. We succeeded in reproducing the occurrence and non-occurrence of temporary WiEsL intensification in 2009 and 2011, respectively, observed by an ionosonde at Kokubunji, Japan, although day-to-day variations in WiEsL intensity were not reproduced well. Evidently, the temporary WiEsL intensification is attributed to vertical ion convergence (VIC) intensification at altitudes of 100–120 km between 4 and 8 local time (LT) and particularly after 15 LT. The VIC intensification is caused primarily by the vertical wind shears of SW2 tides, westward propagating semi-diurnal tides with wavenumber 2. The SW2 intensification is driven by the major SSW in January–February 2009. Additionally, 6–8-day planetary waves can also affect the WiEsL intensification superposed on the SW2 amplification effects.

Keywords Sporadic E layer, Ionosphere, Simulation, Atmospheric tides, Sudden stratospheric warming, Mid-laitudes

*Correspondence:
Satoshi Andoh
andoh@nict.go.jp
Full list of author information is available at the end of the article

Graphical Abstract

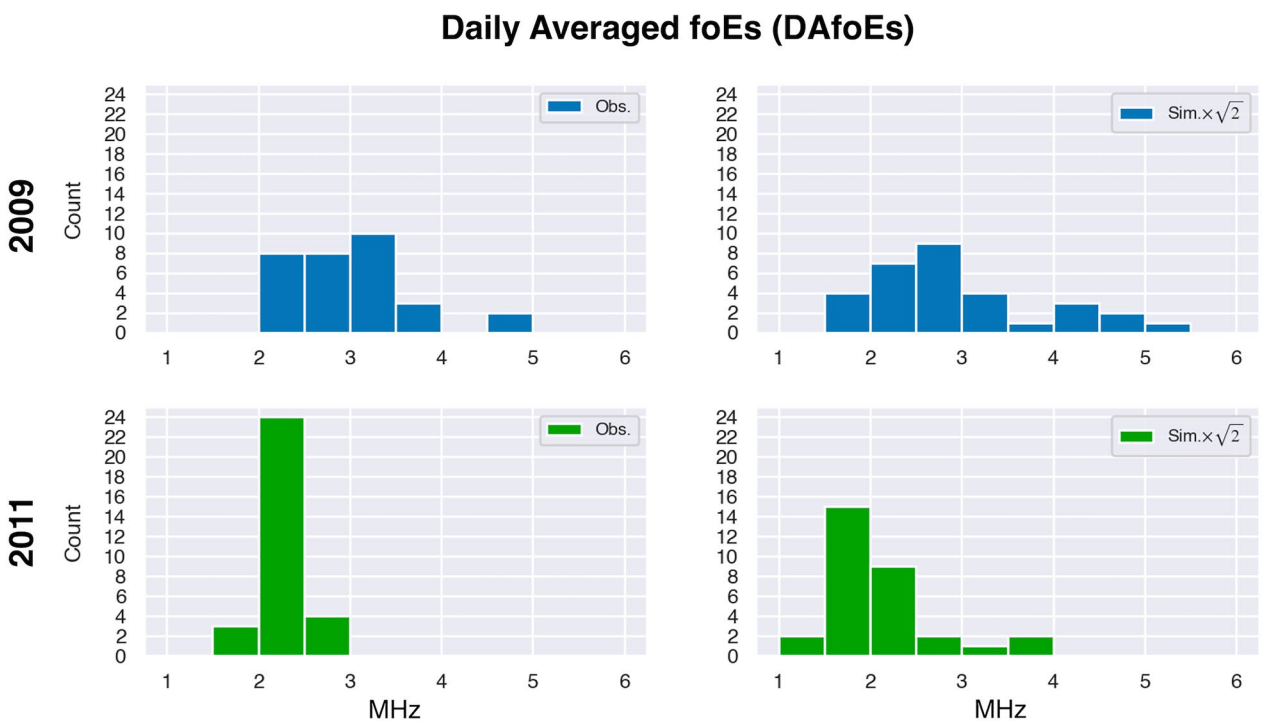

Introduction

Layering structures appearing in the ionospheric *E* region are called sporadic E layers (EsLs). The EsLs primarily comprise long-living metal ions such as Fe^+, Mg^+, and Ca^+ (Kopp 1997). The metal ions are supplied into the lower ionosphere by meteor injections (e.g., Carrillo-Sánchez et al. (2015); Plane et al. (2015)). It is well established that the vertical shears of horizontal winds gather metal ions vertically and form thin EsLs, which is called the wind shear theory (Whitehead 1961; Axford 1963; Haldoupis 2011). The vertical horizontal-wind shears are primarily driven by the semi-diurnal and diurnal tides (e.g., Christakis et al. (2009); Haldoupis (2011)). This implies connections between the EsLs and lower atmospheric variations through tidal variations.

EsL intensity is minimal in winter (e.g., Wu et al. (2005); Haldoupis et al. (2007); Arras et al. (2008); Chu et al. (2014); Shinagawa et al. (2017); Arras and Wickert (2018)). The minimum wintertime EsL (WiEsL) intensity is partially due to the background metal ion distributions (e.g., Haldoupis et al. (2007); Chu et al. (2014); Yu et al. (2021); Wu et al. (2021)). Meteor injections into the lower ionosphere are considered to influence the background metal ion distributions (Haldoupis et al. 2007; Chu et al. 2014; Yeh et al. 2014). Recent global simulations indicated that inter-hemispheric ion transport is crucial for metal ion distribution variations (Yu et al. 2021; Wu et al. 2021). Another possible factor for the WiEsL intensity minimum is vertical wind shear weakening (Chu et al. 2014; Yeh et al. 2014; Shinagawa et al. 2017; Yu et al. 2019; Shinagawa et al. 2021). Shinagawa et al. (2021) demonstrated that the vertical ion convergence (VIC) driven by wind shears correlates with seasonal EsL occurrences deduced from radio occultation observations.

Despite the winter minimum of EsL intensity, temporary intensifications of WiEsLs have been observed since the 1950 s at the latest (Smith 1957; Finney and Smith 1960). Temporary WiEsL intensifications persist for 10–30 days and are considered to be caused by major meteor showers, which increase the background metal ion density (Whitehead 1989; Chandra et al. 2001; Maruyama et al. 2003; Jacobi et al. 2013). However, temporary WiEsL intensifications have not always been observed in conjunction with major meteor showers (Maruyama et al. 2003; Yeh et al. 2014; Shinagawa et al. 2021). For example, in Fig. 1 of Shinagawa et al. (2021), temporary WiEsL intensifications were observed around 40 day of year (DOY) and 340 DOY in 2009 at Kokubunji,

Japan. The period of intensification around 340 DOY corresponds well to the Geminid meteor shower, which occurs annually, peaking in activity around December 13. In contrast, the period of intensification around 40 DOY does not correspond to the main meteor shower periods during wintertime, that is, the Geminid and Quadrantid meteor shower periods (the peak of the Quadrantid meteor shower occurs around January 3). Previous studies have shown that EsL intensifications occur with a delay of 2–3 days or 1–2 weeks from major meteor showers (Sinno 1980; Jacobi et al. 2013). However, the WiEsL intensification around 40 DOY in 2009 occurred more than two weeks after the peak of the Quadrantid meteor showers. It should be noted that recent studies demonstrated that the sporadic micrometeoroids with approximately 10^{-11}–10^{-4} g are the main source of metal ions in the ionosphere rather than meteor showers (Plane 2012; Rapp et al. 2012; Plane et al. 2015). Thus, EsL intensity does not necessarily relate to the major meteor showers.

Jacobi et al. (2013) suggested that factors other than meteor showers, such as wind shear variations, are required to control temporary WiEsL intensifications. However, previous studies have shown that, on average, vertical wind shears are weak during the wintertime (Yeh et al. 2014; Shinagawa et al. 2017; Yu et al. 2019; Luo et al. 2021). The weak vertical wind shears cannot account for temporary WiEsL intensifications. Thus, the physical mechanisms of the WiEsL intensification around 40 DOY in 2009 are still unknown.

A sudden stratospheric warming (SSW) event occurred at the northern high latitudes in late January 2009 (e.g., Pedatella and Forbes (2010); Pedatella et al. (2014); Butler et al. (2017)). SSW events can change wind distributions not only at high latitudes but also at mid and low latitudes (Liu and Roble 2002; Jin et al. 2012; Tang et al. 2020). Tang et al. (2020) demonstrated that midlatitude EsL intensity can be affected by the lunar tides, which are enhanced by SSW events. However, links between EsL intensity and SSW events through wind distributions have not been examined extensively. The period of an SSW event in 2009 corresponds well to the WiEsL intensification around 40 DOY as observed by the ionosonde at Kokubunji. This implies a possible link between the SSW event and WiEsL intensification in 2009.

Recently, we have developed a local ionospheric model including metal ion transport and chemical processes. The model is coupled with the neutral winds of the ground-to-topside model of atmosphere and ionosphere for aeronomy (GAIA model) (Jin et al. 2011). The GAIA model succeeded in reproducing many features of the major SSW event in 2009 (Jin et al. 2012). Thus, we can simulate EsL intensity variations under the wind changes caused by the SSW event in 2009. Using the model, in this study, we aimed to demonstrate the physical mechanisms of the temporary WiEsL intensification observed in 2009. EsL simulations

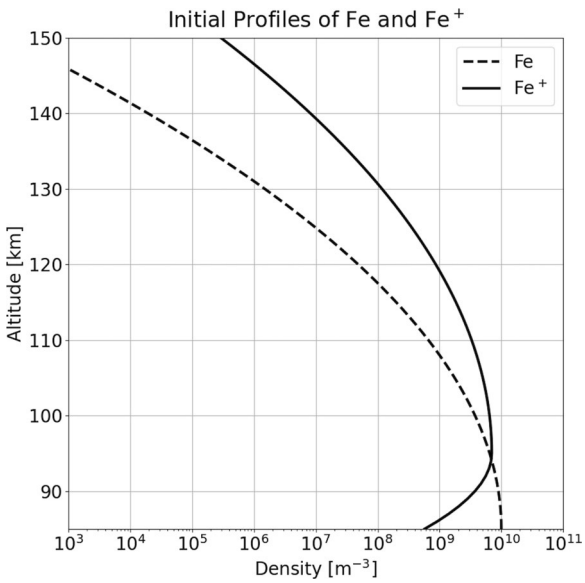

Fig. 1 Initial profiles of Fe and Fe^+ densities used as an initial condition

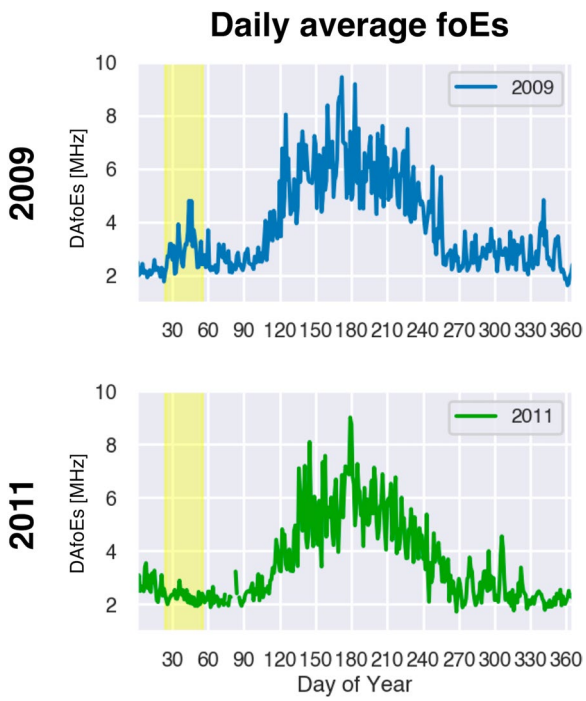

Fig. 2 Daily average foEs as observed by the ionosonde at Kokubunji in 2009 (upper panel) and 2011 (lower panel). The ranges in yellow indicate the periods from 24 DOY (January 24) to 54 DOY (February 23) when the temporary WiEsL intensification was observed in 2009

were performed, and the simulation results were compared with the ionosonde observations at Kokubunji, Japan.

Model and data

We utilized the same ionospheric model developed by Andoh et al. (2020), excluding the metal ion species and a location of the numerical domain. Details of the numerical model were described by Andoh et al. (2020, 2022). The center of the numerical domain was set to Kokubunji with the geographic coordinates of 35.7°N and 139.5°E and the geomagnetic coordinates of 26.8°N and 151.1°E. We used Fe^+ as a proxy for metal ions in the model because Fe^+ is one of the most abundant ions in the EsLs (Kopp 1997). The chemical reactions associated with Fe and Fe^+ were obtained from Chu and Yu (2017), and their reaction numbers in Chu and Yu (2017) were R1, R3–R5, R7–R8, and R11–R17 (Rutherford et al. 1972; Nahar et al. 1997; Bautista et al. 1998; Helmer et al. 1998; Plane et al. 1999; Vondrak et al. 2006; Woodcock et al. 2006; Bones et al. 2016). The initial Fe and Fe^+ densities were estimated from Feng et al. (2013) using the following equations:

$$N_{Fe}(z) = 10^{10} \times \exp\left\{-\frac{(z-85)^2}{230}\right\}, \tag{1}$$

$$N_{Fe^+}(z) = \begin{cases} 10^9 \times \exp\left\{-\frac{(z-95)^2}{40}\right\} & \text{(below 95 km)}, \\ 10^9 \times \exp\left\{-\frac{(z-95)^2}{300}\right\} & \text{(above 95 km)}, \end{cases} \tag{2}$$

where z is the altitude [km]. These profiles are shown in Fig. 1. They were uniformly distributed in the horizontal domain as an initial condition. To remove the initial transients, the simulations were run for 48 h, and the simulation results of the first 24 h were discarded.

The geomagnetic fields were taken from the IGRF-12 model (Thébault et al. 2015). The neutral species densities, except Fe, and neutral temperature were constrained using the NRLMSISE-00 model (Picone et al. 2002). The Ap and F10.7 indices for each simulated day were obtained from the World Data Center for Geomagnetism in Kyoto (http://wdc.kugi.kyoto-u.ac.jp/wdc/Sec3.html) and NOAA/NCEI (https://www.ngdc.noaa.gov/stp/spaceweather.html), respectively.

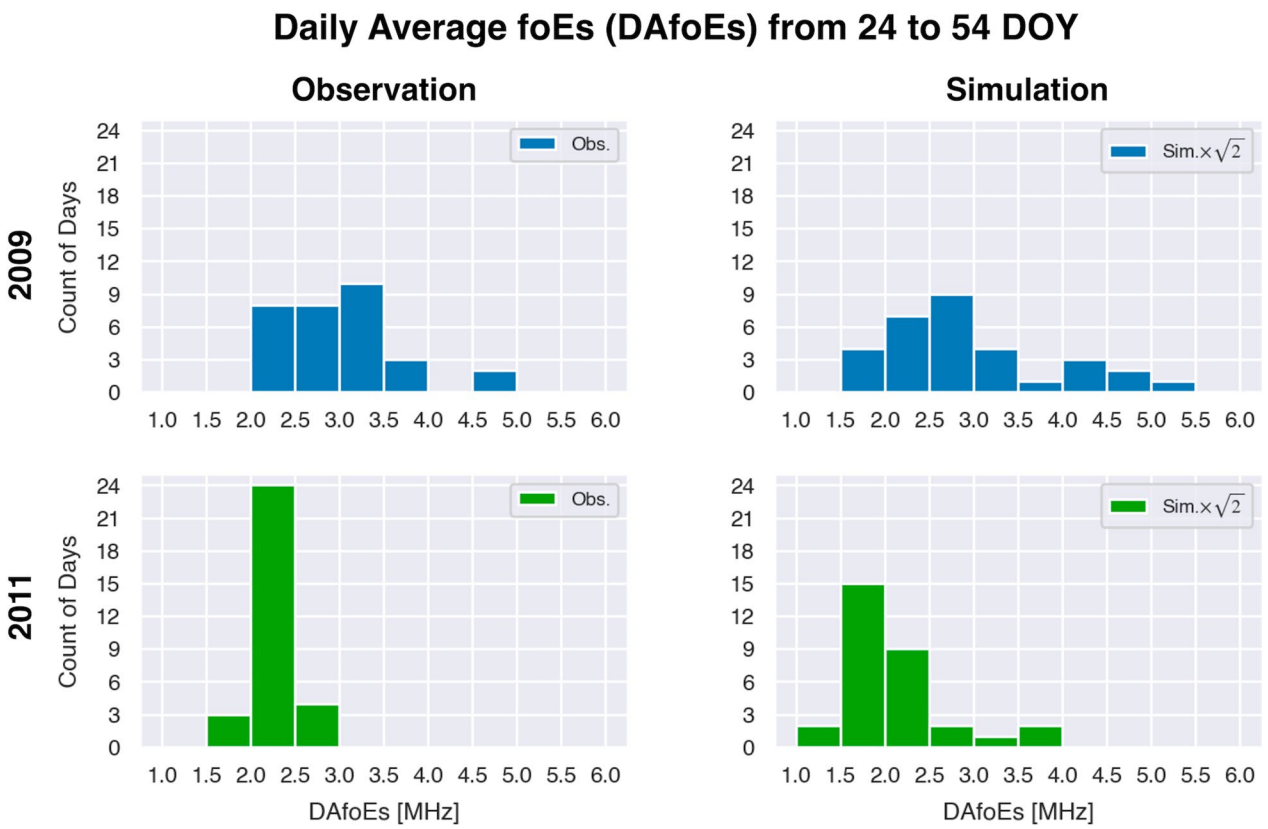

Fig. 3 Histograms of the observed (first column) and simulated (second column) DAfoEs values at Kokubunji from 24 to 54 DOY in 2009 and 2011. The vertical axis represents the counts of days, and the horizontal axis represents the intensity of DAfoEs.

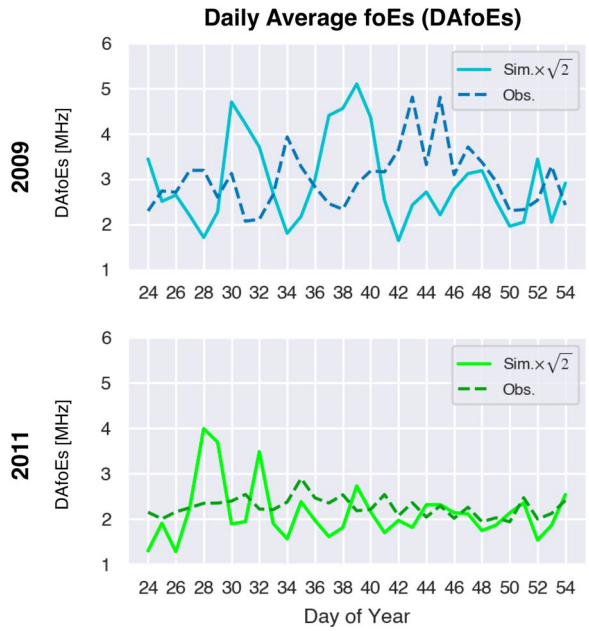

Fig. 4 Day-to-day variations in the simulated and observed DAfoEs values from 24 to 54 DOY in 2009 and 2011. The solid and dashed lines indicate the simulated and observed DAfoEs variations, respectively

The neutral wind velocity was obtained from the GAIA model (Jin et al. 2011). The atmospheric portion of the GAIA model below 40 km is constrained with meteorological reanalysis data via a nudging method (Jin et al. 2012). This method enables the GAIA model to generally reproduce the neutral winds including the atmospheric tides that propagate from the lower atmosphere to the ionosphere (Miyoshi et al. 2017). Previously, we used neutral winds as the input for EsL simulations and succeeded in reproducing the day-to-day variations in the low- and midlatitude EsLs for the first time (Andoh et al. 2020, 2022). The GAIA-modeled neutral winds were linear-interpolated in the vertical direction and spline-interpolated in the horizontal direction to adopt the grid spacing of our ionospheric model.

In this study, we utilized foEs ($\approx 9\sqrt{N_e}$; N_e is the electron density) observed by an ionosonde located at Kokubunji, Japan. The ionosonde observation is operated by the National Institute of Information and Communications Technology in Japan (https://wdc.nict.go.jp/IONO/HP2009/ISDJ/index-E.html). Figure 2 shows the daily average foEs (DAfoEs) observed by the ionosonde at Kokubunji in 2009 (upper panel) and 2011 (lower panel). The ranges in yellow indicate the periods of WiEsL intensification in 2009. We chose 2011 as a reference year of WiEsL intensity variations because no major SSW events occurred (Butler et al. 2017) and DAfoEs variations were not perturbed significantly. The DAfoEs values in both 2009 and 2011 exhibit 6–8-day cycles and, in general, summer maximum and winter minimum. However, within the ranges in yellow, DAfoEs values increase in 2009 only, which is the WiEsL intensification. No major meteor shower occurs around these periods in this range annually. Hence, the temporary WiEsL intensification in the range in yellow cannot be explained by the major meteor showers.

To elucidate the mechanisms of the temporary WiEsL intensification in 2009, we conducted month-long EsL simulations from 24 DOY (January 24) to 54 DOY (February 23) in 2009 and 2011. As shown in Fig. 2, the intensification of WiEsLs occurred evidently during the period in 2009, but not in 2011. To calculate foEs from the simulation, we obtained the altitudes at which the metal ion density was maximum at each local time, and the simulated foEs was deduced from the electron density at the altitudes. The simulated foEs was multiplied by $\sqrt{2}$ because our model included only Fe^+, but not Mg^+. Previous observations have shown that the EsL density approximately equals the summation of Fe^+ and Mg^+ densities (Kopp 1997). In the EsLs, the Mg^+ density was roughly equivalent to Fe^+ density. Thus, the simulated EsL density should be roughly doubled, and the simulated foEs should be $\sqrt{2}$ times.

Results and discussion

Figure 3 shows the histogram comparison between the observed (first column) and simulated (second column) DAfoEs values at Kokubunji from 24 to 54 DOY in 2009 and 2011. The vertical axis represents counts of days, and the horizontal axis represents the intensity of DAfoEs. For instance, the observed DAfoEs in 2011, in the lower-left panel of Fig. 3, are between 2.0 and 2.5 MHz in 24 days. The DAfoEs values in 2009 were distributed between 2.0 and 5.0 MHz in the observation and between 1.5 and 5.5 MHz in the simulation. In 2011, the DAfoEs values were generally below 3.0 MHz both in the observation and simulation. Most of the DAfoEs values in 2011 were around 2.0 MHz. A comparison of the simulated/observed DAfoEs values in 2009 with those in 2011 showed that the simulated/observed DAfoEs values in 2009 were higher. The observed and simulated DAfoEs values higher than 3.0 MHz appeared in 15 and 11 days out of 31 days in 2009, but in only 0 and 3 days out of 31 days in 2011. Thus, more intense EsLs occurred both in observations and simulations of 2009 than in those of 2011, which is the WiEsL intensification. The simulation successfully reproduced the occurrence and non-occurrence of temporary WiEsL intensification in 2009 and 2011, respectively.

However, the day-to-day variations of DAfoEs values were not reproduced well in the simulation, as shown in

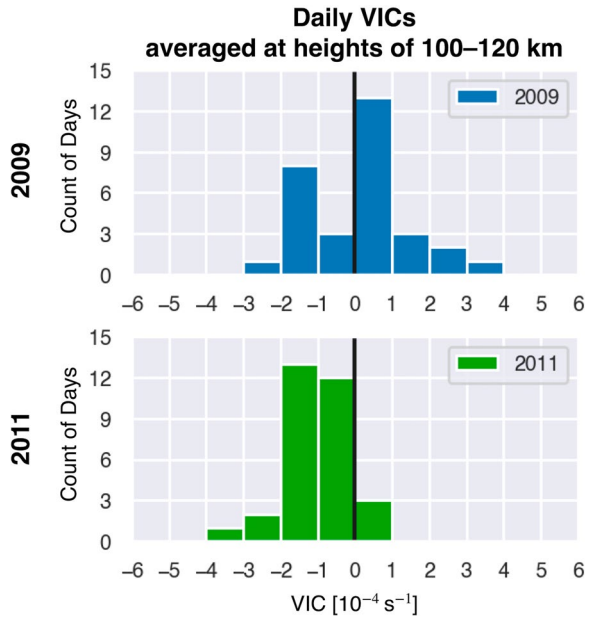

Fig. 5 Daily VICs averaged between 100 and 120 km from 24 to 54 DOY in 2009 (upper panel) and 2011 (lower panel)

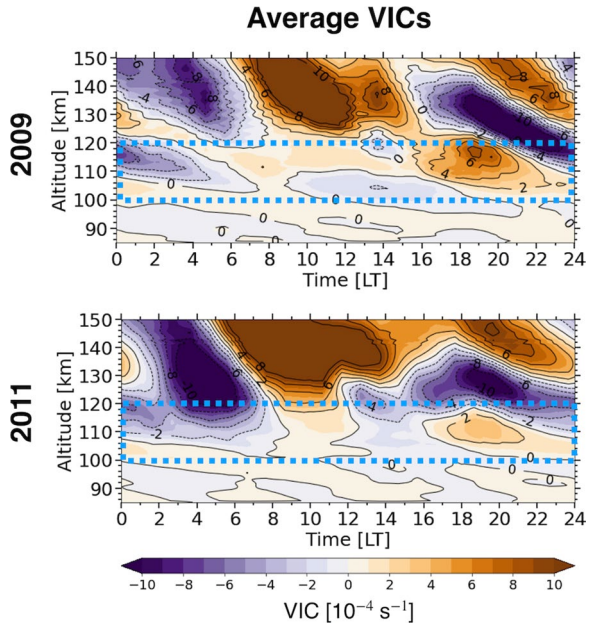

Fig. 6 VIC variations averaged between 24 and 54 DOY in 2009 (upper panel) and 2011 (lower panel). The altitudes of 100–120 km are surrounded by blue dashed lines

Fig. 4. Figure 4 shows the day-to-day DAfoEs variations in the observation (dashed lines) and simulation (solid lines) in 2009 and 2011. Both observations and simulations showed 6–8 day cycle DAfoEs variations in the two years. Moreover, the DAfoEs was perturbed and amplified more severely in 2009 than in 2011, which shows the temporary WiEsL intensification. However, day-to-day DAfoEs variations in the simulations differ from those in the observations. As indicated by Andoh et al. (2021), the EsL intensity observed by the ionosondes (i.e., DAfoEs) is influenced by the horizontal EsL movements and structures. Hence, in the ionosonde observations, the spatial EsL variations can be confused with the temporal EsL variations. The ionosondes cannot completely observe the day-to-day variations in EsL intensity, and it is reasonable that the day-to-day DAfoEs variations in the simulation were not consistent with those observed by the ionosonde. We need both 3D observations and simulations to investigate the day-to-day EsL intensity variations. Thus, in this study, we did not comprehensively analyze these factors but rather investigated the average, weeks-long EsL features during the temporary WiEsL intensification period.

It should be pointed out that uncertainties in the neutral winds of the GAIA model, used for inputs, could also cause discrepancies in day-to-day variations in DAfoEs between the observations and simulations. The GAIA model does not fully reproduce atmospheric gravity waves because of its coarse grid spacing. Atmospheric gravity waves are considered to generate day-to-day variations in atmospheric tides (Miyoshi and Fujiwara 2008; Yiğit and Medvedev 2017). Furthermore, the stratospheric and mesospheric winds in the GAIA model could modulate the thermospheric tides propagating from the lower atmosphere, which may cause disagreements between simulated tides and real ones in the lower thermosphere. These uncertainties could affect day-to-day variations in the simulated tides in the lower thermosphere, and influence day-to-day variations in the simulated EsLs in this study.

We then investigated the mechanisms underlying the temporary WiEsL intensification in the simulation for 2009. In the present simulation, we did not incorporate meteor injections. The simulated temporary WiEsL intensification in 2009 occurred as a result of the VIC variations due to neutral winds. We further examined when the VIC variations caused the temporary intensification of the simulated WiEsLs and at which altitudes. The VIC can be calculated as follows:

$$VIC = -\frac{\partial w_i}{\partial z}, \tag{3}$$

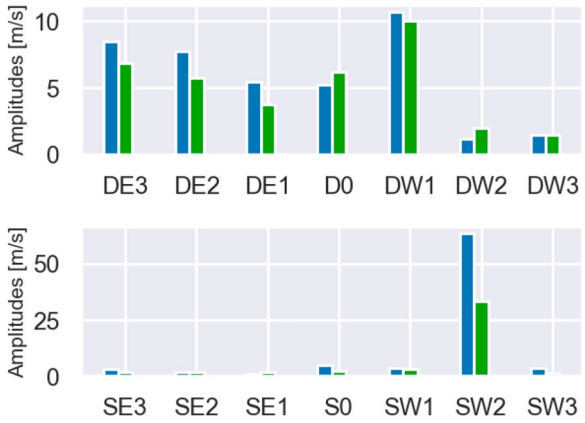

Fig. 7 Extracted amplitudes of the diurnal tides (upper panel) and semi-diurnal tides (lower panel) with wavenumbers from −3 to +3 at 35.7°N and 110 km altitude between 24 and 44 DOY. The blue and green bars represent the tidal amplitudes for 2009 and 2011, respectively

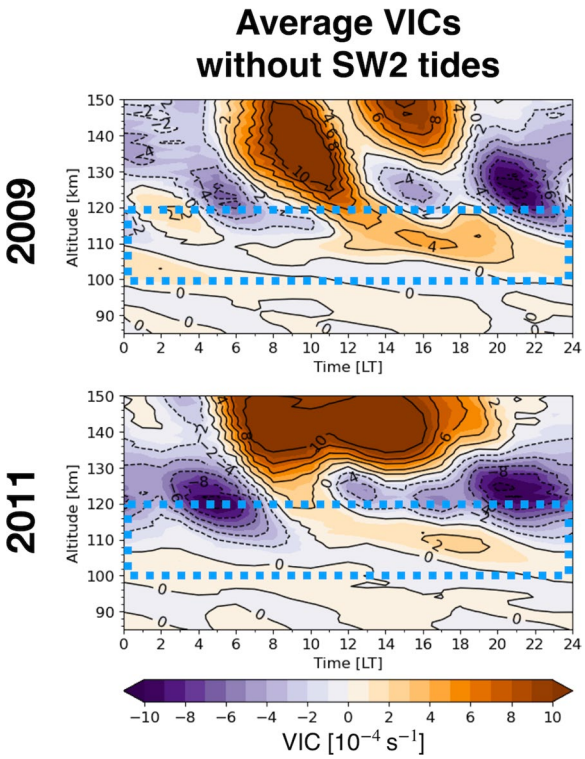

Fig. 8 VIC variations averaged between 24 and 54 DOY in 2009 (upper panel) and 2011 (lower panel) without SW2 tides. The altitudes of 100–120 km are surrounded by blue dashed lines

where w_i is the vertical ion velocity, ξ is the ratio of the ion-neutral collision frequency to the ion gyrofrequency, $\vec{b}$ is the unit vector of the geomagnetic fields, $\vec{V}_n$ is the neutral wind velocity, and $\vec{e}_z$ is the vertical unit vector. The positive VIC indicates enhancements in the ion density and vice versa.

EsL intensity is related to VIC, especially below 120 km altitude (Shinagawa et al. 2017; Yu et al. 2019; Shinagawa et al. 2021; Sobhkhiz-Miandehi et al. 2022; Yamazaki et al. 2022). Furthermore, at midlatitudes, the diurnal tides that can form EsLs below 100 km are weak, and EsLs are not affected significantly by VIC below 100 km (Andoh et al. 2020; Yamazaki et al. 2022). Therefore, EsL intensity at mid-latitudes is considered to be affected by VICs, especially between 100 and 120 km altitudes. Figure 5 shows the daily VIC averaged at the heights of 100 and 120 km in 2009 and 2011 (upper and lower panels, respectively) from 24 to 54 DOY. The daily and height-averaged VICs tended to be positive in 2009, compared with those in 2011. With these higher VICs in 2009, the EsL intensity was higher in 2009 than in 2011.

Figure 6 shows the vertical gradients of vertical ion velocity, that is, VICs averaged over the simulation period in 2009 and 2011. We note that EsLs appear in the positive VIC regions. In Fig. 6, the periodic VIC variations are observed between 100 and 120 km in both years. At the heights of 100–120 km, clear differences in the positive VIC regions in 2009 and 2011 appeared between 4 and 8 LT and particularly after 15 LT. Between 4 and 8 LT, the positive VIC regions descended from 120 to 110 km in 2009 but not in 2011. After 15 LT, the VIC neared 8.0×10^{-4} s^{-1} in 2009 and neared 3.0×10^{-4} s^{-1} in 2011. The VIC differences in each year, particularly the VIC enhancement after 15 LT, caused a stronger VIC between 100 and 120 km altitude in 2009 than in 2011. The semi-diurnal tides drove the morning and evening VIC intensification, and the diurnal tides drove the evening VIC intensification. Consequently, the evening intensification was stronger than the morning intensification.

Previous studies have revealed that the vertical wind shears in the lower thermosphere are generally weak during wintertime (e.g., Shinagawa et al. (2017); Yu et al. (2019); Yamazaki et al. (2022)). However, we showed that wintertime vertical wind shears could be intensified, as shown in Fig. 6. We then investigated which diurnal and semi-diurnal tides drive the VIC intensification in 2009. The semi-diurnal and diurnal tides with wavenumbers from −3 to +3 were extracted from the neutral winds of

$$w_i = \left(\frac{1}{1+\xi^2}(\vec{V}_n \cdot \vec{b})\vec{b} + \frac{\xi}{1+\xi^2}\vec{V}_n \times \vec{b} + \frac{\xi^2}{1+\xi^2}\vec{V}_n \right) \cdot \vec{e}_z, \quad (4)$$

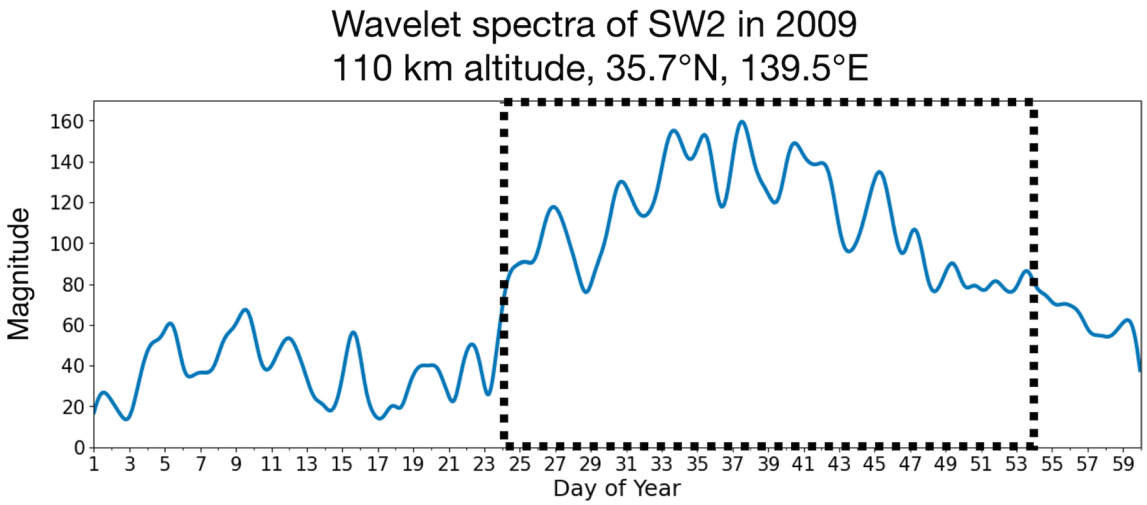

Fig. 9 Wavelet spectra of SW2 tides in 2009 at 110 km altitude, 35.7°N, and 139.5°E

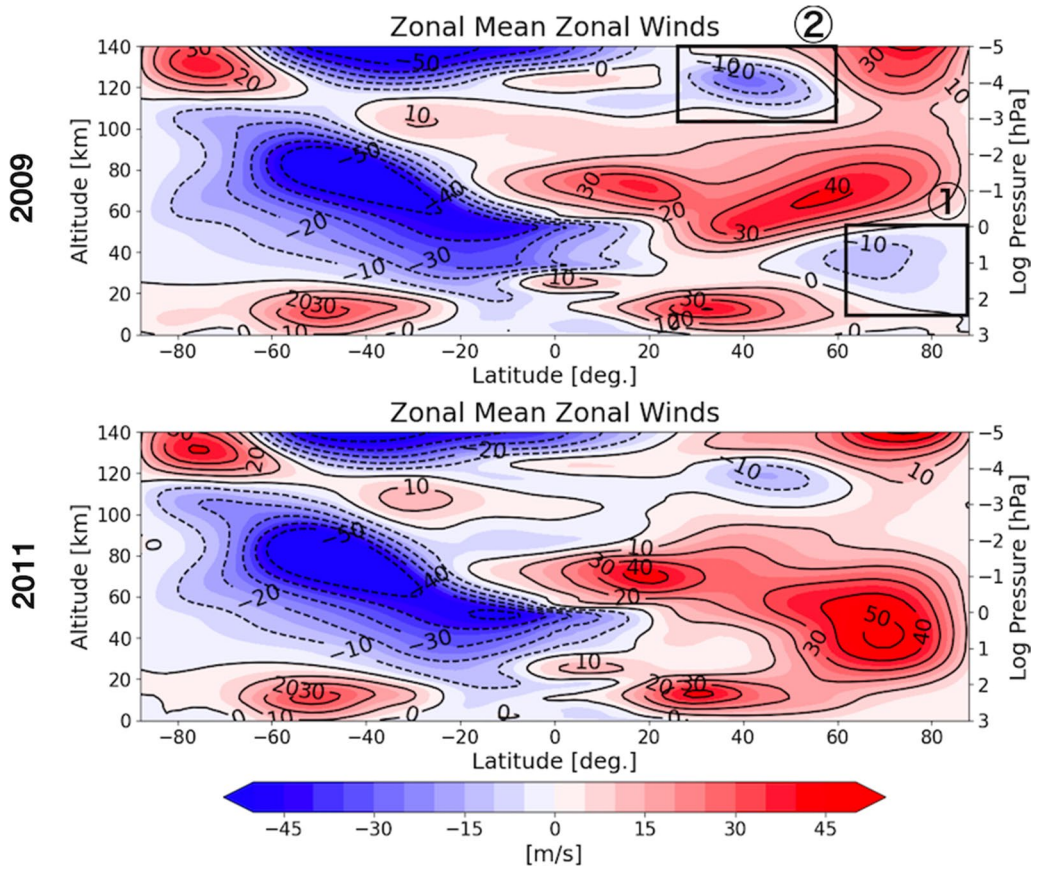

Fig. 10 Altitude–latitude cross-section of zonal-mean zonal winds (ZMZWs) between 2009 and 2011 from the surface to the ionospheric E region. The ZMZWs were averaged during the simulation period (24–54 DOY). The red and blue colors indicate the eastward and westward winds, respectively.

the GAIA model during the simulation period, from 24 to 54 DOY at 35.7°N and 110 km altitudes. The following fitting function was used in the extraction (e.g., Yamazaki (2018); Griffith and Mitchell (2022)):

$$\sum_{T,s} A_{T,s} \cos\left\{2\pi\left(\frac{t}{T} + s\frac{\lambda}{360}\right) - \phi_{T,s}\right\} + B, \quad (5)$$

where A is the amplitude of the wave, t is the universal time (in days), T is the period of the wave (in days), s is the zonal wavenumber, λ is the longitude (in degrees), ϕ is the phase of the wave, and B is the background value. In this study, abbreviated expressions were used for the atmospheric tidal components. For example, SW2 tides mean westward propagating semi-diurnal tides with wavenumber 2, and DE1 tides mean eastward propagating diurnal tides with wavenumber 1.

Figure 7 shows the extracted amplitudes of diurnal (upper panel) and semi-diurnal (lower panel) tidal components with wavenumbers from −3 to +3 at 35.7°N and 110 km altitudes. The blue and green bars represent the tidal amplitudes in 2009 and 2011, respectively. Note that the vertical axis range differs in each panel. In the upper panel, there are no diurnal tidal components showing evident enhancement only in 2009. The amplitudes of the diurnal components are generally lower than 10 m/s in both years. The DE1, DE2, and DE3 tides are greater in 2009 than in 2011. In the lower panel, SW2 tides, the migrating semi-diurnal tides, are the most dominant components. The SW2 amplitudes were 63 and 33 m/s in 2009 and 2011, respectively. The other semi-diurnal components show amplitudes lower than 10 m/s. The SW2 amplification is more significant than DE1, DE2, and DE3 amplifications. The SW2 amplitudes are greatest in Fig. 7, and SW2 tides amplify particularly in 2009. Thus, SW2 tides are the most plausible drivers of VIC intensification in 2009.

Fig. 8 shows VIC variations averaged between 24 and 54 DOY in 2009 (upper panel) and 2011 (lower panel) without SW2 tides. The altitudes of 100–120 km are surrounded by blue dashed lines. At the altitudes of 100–120 km, the positive VIC at the LTs of 6–9 and 16–22 h

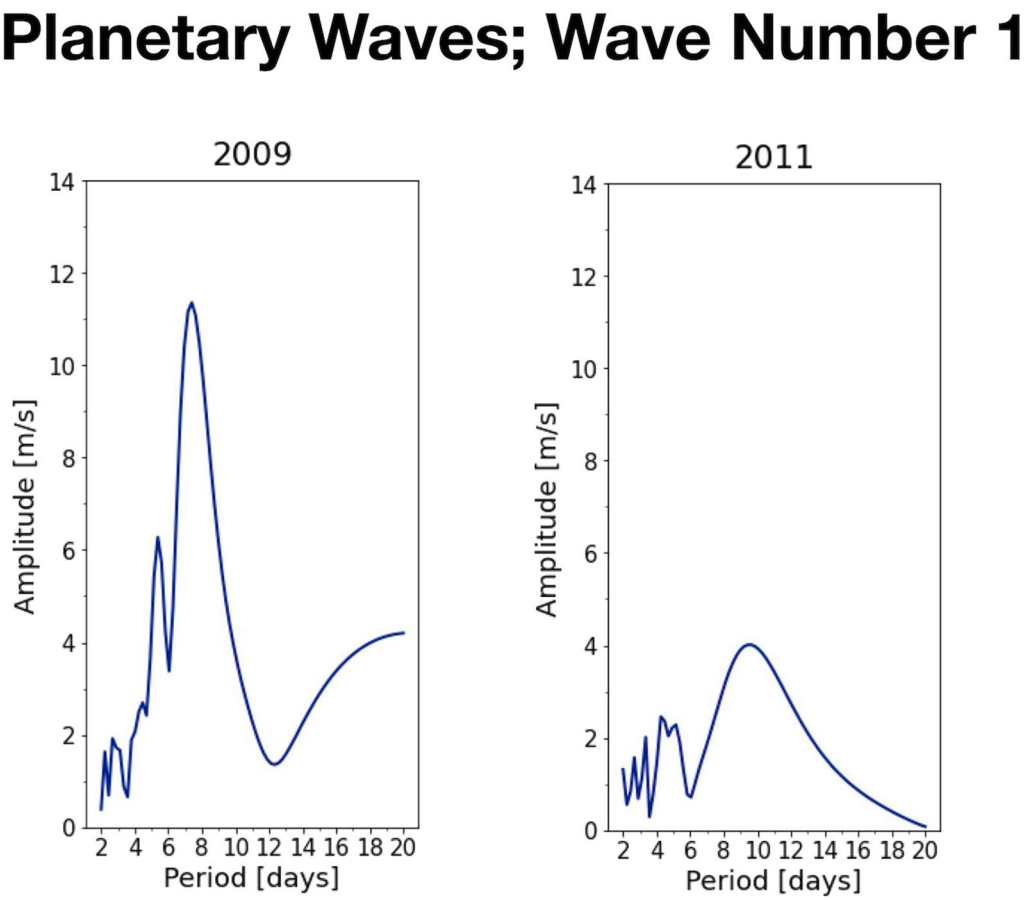

Fig. 11 Amplitudes of the zonal PWs with wave number 1 from 24 to 54 DOY at 110 km altitude and 35.7°N in 2009 (left panel) and 2011 (right panel)

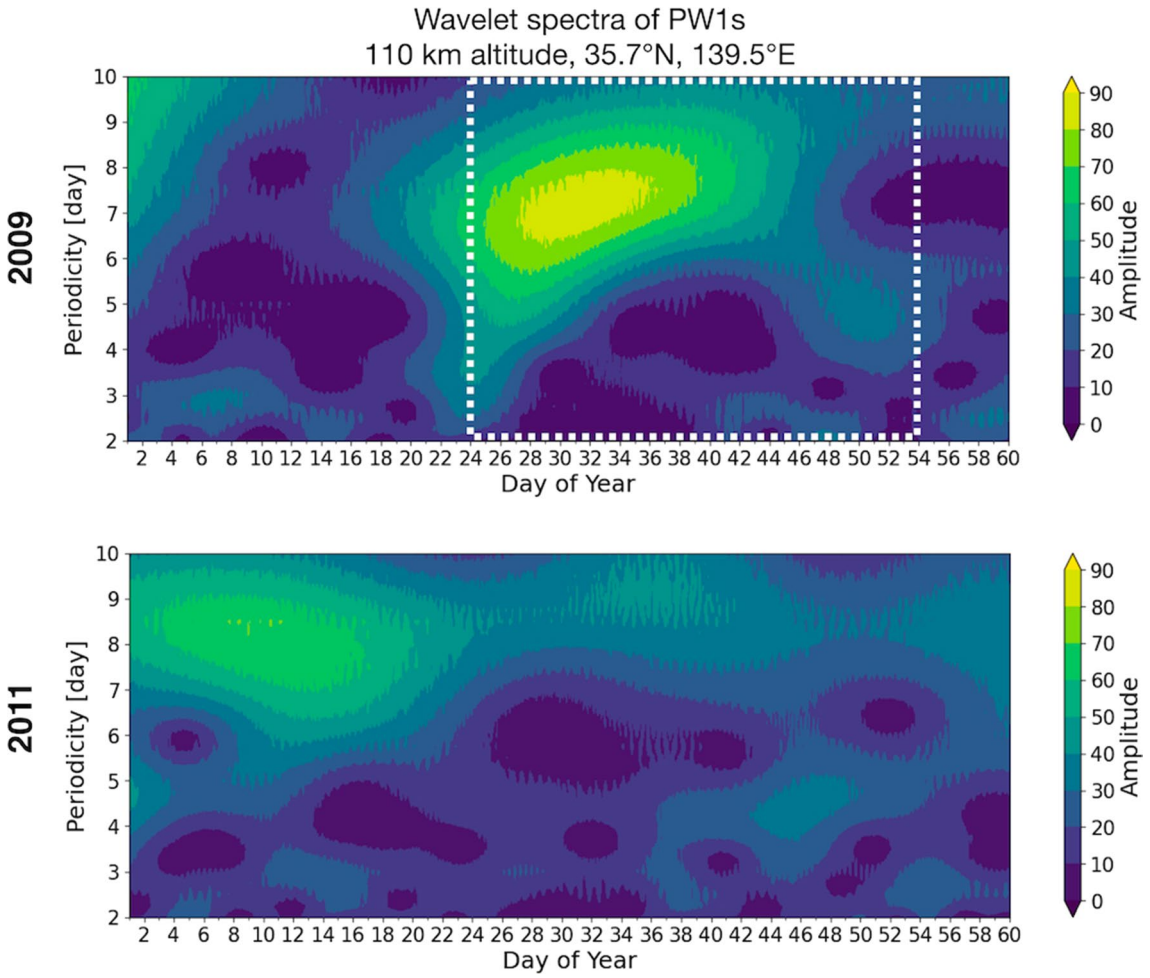

Fig. 12 Wavelet spectra of PW1s with 2–10-day periodicity in 2009 (upper panel) and 2011 (lower panel) at 110 km altitude, 35.7°N, and 139.5°E

in 2009 is weaker as compared to Fig. 6. The intense VIC, which was ~8.0×10^{-4} s^{-1} between 18 and 19 LT in Fig. 6 for 2009, weakens to ~3.0×10^{-4} s^{-1} and becomes compatible with that for 2011 without SW2 tides, as shown in Fig. 8. This indicates that SW2 tides are the most important tidal component for VIC intensification at the altitude and LT ranges.

A possible mechanism of the SW2 tide amplification is zonal-mean zonal wind (ZMZW) variations in the high-latitude stratosphere due to the major SSW event in 2009 (e.g., Pedatella and Forbes (2010); Jin et al. (2012); Pedatella et al. (2014)). The ZMZWs in the wintertime high-latitude stratosphere can change from eastward to westward owing to SSW events. Jin et al. (2012) demonstrated that the midlatitude SW2 tides can be amplified more significantly as the inter-hemispheric asymmetry of the ZMZW direction becomes largely reduced in the stratosphere. Figure 9 shows daily variations of SW2 amplitudes from 1 to 59 DOY in 2009, as obtained by the wavelet analysis using the Morlet mother function. The simulation period, 24–54 DOY, is encircled by a dashed square. The SW2 amplitudes begin being amplified at 24 DOY, the time when the major SSW event occurred (Jin et al. 2012; Pedatella et al. 2014). SW2 amplitudes have their peak at around 38 DOY and decrease gradually after 38 DOY. The SW2 amplitude variations correspond generally to simulated DAfoEs variations in Fig. 4. Figure 10 shows the ZMZWs in the altitude and latitude cross sections averaged from 24 to 54 DOY in 2009 and 2011. These ZMZWs were obtained from the neutral winds of the GAIA model. As indicated by black square 1, the ZMZWs are generally westward in the northern stratosphere at high latitudes in 2009, but eastward in 2011. The westward direction of the ZMZWs is a typical feature of major SSW events (e.g., Liu and Roble (2002); Jin et al. (2012); Koushik et al. (2022)). The inter-hemispheric asymmetry of the ZMZW direction in Fig. 10 is more evident in 2011 than in 2009. Therefore, according to Jin et al. (2012), SW2 tides can more significantly amplify in 2009 than in 2011, which is consistent with the SW2

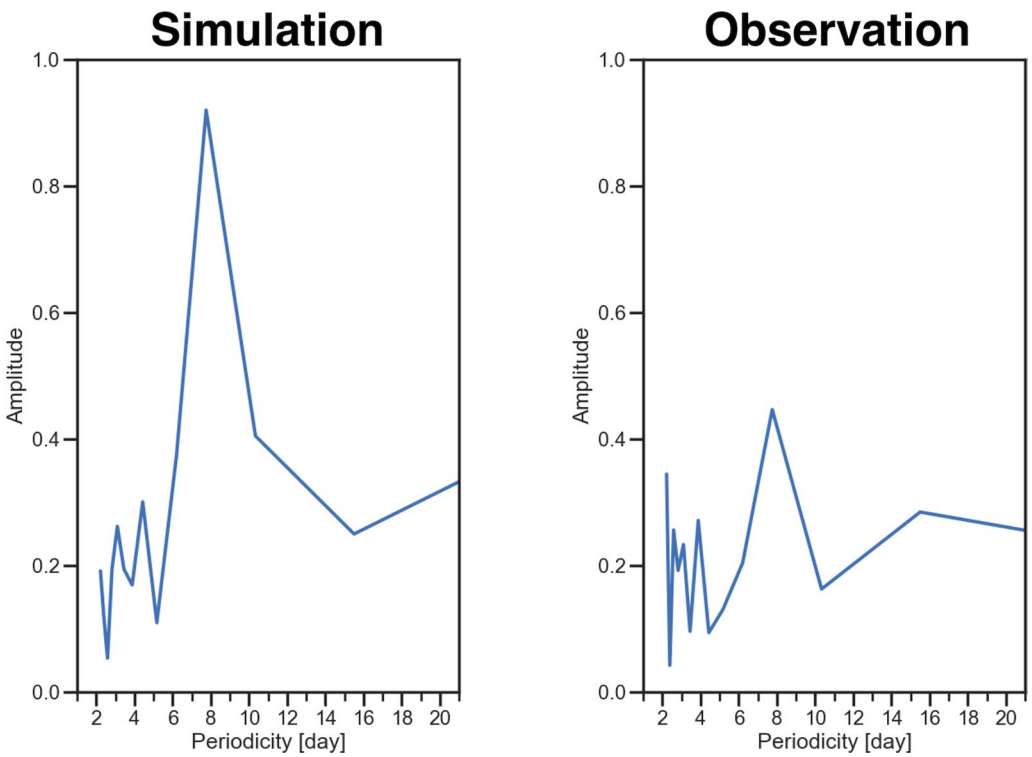

Fig. 13 Fourier amplitudes for simulated DAfoEs (left column) and observed DAfoEs (right column) from 24 to 54 DOY in 2009 at 35.7°N and 139.5° E

amplitudes of the midlatitude ionosphere in the present simulation shown in Fig. 7. Thus, the ZMZW variations triggered by SSW events are a possible factor for the midlatitude SW2 amplification and WiEsL intensification in the simulation for 2009.

The perturbed behaviors of DAfoEs during the WiEsL intensification event in the simulation, as shown in Fig. 4, were attributed to tidal modulations by planetary waves (PWs). Tidal modulations by PWs are important for day-to-day variations of the tides in the ionosphere (e.g., Forbes (1996); Liu et al. (2007); Chang et al. (2011); Pedatella et al. (2012a)). We extracted zonal PWs from the neutral wind data using the same method as that in the tidal extraction. We found that the zonal PW amplitudes of wave number 1 (PW1) differed significantly between 2009 and 2011. Figure 11 shows the zonal PW1 amplitudes between 24 and 54 DOY in 2009 (left panel) and 2011 (right panel) at 35.7°N and 110 km altitude where the VIC enhancement occurred. Evidently, the zonal PW1 amplitudes are lower in 2011 than in 2009. The zonal PW1 amplitudes with the 6–8-day periodicity reached more than 10 m/s in 2009 but not in 2011.

Figure 12 shows the wavelet spectra of zonal PW1s with 2–10-day periodicity from 1 to 59 DOY in 2009 (upper panel) and 2011 (lower panel) at 110 km altitude and 35.7°N, obtained using the Morlet mother function. The simulation period is emphasized by the dashed square. The amplification of 6–8-day PWs can be observed only in 2009 before 42 DOY, the time when the evident temporary WiEsL intensification occurred in the simulation as shown in Fig. 4. Therefore, the SW2 tides can be modulated by the amplified 6–8-day PWs in 2009 during the temporary WiEsL intensification event. We note that the 6–8-day periodicity in foEs variations was previously reported by various groups (e.g., Haldoupis and Pancheva (2002); Pancheva et al. (2003a); Zuo and Wan (2008)). The 6–8-day PWs can be an important factor for WiEsL intensification in 2009. The Fourier analysis was performed for the observed and simulated DAfoEs in 2009 of Fig. 4, and shown in Fig. 13. The 6–8-day oscillations are evident in both the observation and simulation of 2009. These Fourier amplitudes for the simulated DAfoEs correspond well to the amplitudes of PW1s in Fig. 7. Thus, EsL intensity can be influenced by the 6–8-day PW1s in the WiEsL intensification in 2009.

The PW amplification in 2009 is likely due to the strong westward ZMZWs in the ionospheric E region, as shown in black square 2 in Fig. 10. Some PWs in the ionosphere are considered to be secondary waves excited by the in situ dissipation of the PW-modulated gravity waves (Forbes 1996; Meyer 1999; Forbes et al. 2018). Secondary PWs can be sustained only in the westward ZMZWs. The stronger westward ZMZWs impose a weaker dissipation on the PWs (Forbes 1995). Hence, the PW signatures in Fig. 11 are more dominant in the ionosphere in 2009, where the stronger westward ZMZWs exist at altitudes between 100 and 140 km encircled by black square 2, than in 2011.

We note that the GAIA model did not include the mechanisms to produce lunar tides, and the temporary WiEsL intensification of the present simulation cannot be ascribed to the lunar tide modulation during SSW events as reported by Tang et al. (2020). The migrating semi-diurnal lunar tides are amplified during SSW events (Pedatella et al. 2012b; Pedatella and Liu 2013), and EsLs are affected by the migrating semi-diurnal lunar tides (Sobhkhiz-Miandehi et al. 2022). To completely understand the connections between EsLs and SSW events, we should conduct global EsL simulations including the lunar tidal effects. Furthermore, the neutral winds of the GAIA model did not include chemical mechanisms of SW2 amplifications owing to ozone density variations in the stratosphere/mesosphere (e.g., Lindzen and Chapman (1969); Pancheva et al. (2003b)). Nevertheless, the present simulation reproduced the occurrence of temporary WiEsL intensification in 2009; thus, these effects on temporary WiEsL intensification might be minor. Further analysis including lunar tide effects during SSW events may be necessary to fully understand the generation mechanisms of WiEsL intensification, which will be addressed in future work.

A recent study on winds in the ionosphere showed that the vertical wind shears reproduced by the global ionospheric model were weaker than the observed shears (England et al. 2022). This may be due to the fact that global ionospheric models with the coarse grid spacing could not resolve small-scale gravity waves (Liu 2017). In the present simulation, we used the neutral winds of the GAIA model, and their vertical wind shears could be weaker than the real ones. Sherman and She (2006) reported that strong vertical wind shears occurred at ~100 km altitude and midlatitudes in winter. These strong vertical wind shears might form intense EsLs in winter and cause temporary WiEsL intensification.

In this study, we used the identical metal ion distributions for 2009 and 2011 as initial conditions. Spatial variations in the background metal ion distributions were not considered. Metal ions might converge locally owing to global wind circulation (Yu et al. 2021; Wu et al. 2021), horizontal convergence driven by PWs (Shalimov and Haldoupis 2002), and meteor injections (Feng et al. 2013). Such local metal ion convergence may control the occurrence and day-to-day variations of temporary WiEsL intensification. Furthermore, PW phase variations can also affect day-to-day EsL variations through tidal modulations.

It is well accepted that the VIC driven by tides is the main driver for EsL formations (Christakis et al. 2009; Haldoupis 2012; Andoh et al. 2022). However, this study scrutinized which LT and altitude VIC affect most significantly WiEsL intensification. Furthermore, relationships between amplified SW2 tides caused by SSWs and EsL intensity have not been reported till now, although the lunar tides are considered to affect EsL intensity (Tang et al. 2020). Our numerical EsL model led these new insights, succeeding in reproducing the WiEsL intensification occurrence in 2009 for the first time.

Summary and conclusions

We employed a regional ionospheric model coupled with the neutral winds of a whole atmospheric model to elucidate the possible mechanisms of the temporary WiEsL intensification in 2009. The period of WiEsL intensification corresponded well to that of the SSW event in 2009, which implied links between EsL intensity and the SSW event.

The simulated EsL intensity variations were compared with the variations observed by an ionosonde at Kokubunji, Japan during a temporary WiEsL intensification period. In the simulation, the temporary WiEsL intensification occurred only in 2009 and not in 2011. The simulation reproduced successfully the occurrence of the temporary WiEsL intensification observed by the ionosonde in Japan, although it did not reproduce well the day-to-day variations in EsL intensity. The temporary WiEsL intensification in 2009 was ascribed to VIC enhancement at altitudes between 100 and 120 km. The simulated VIC strengthened between 4 and 8 LT and particularly after ~15 LT.

Although wintertime vertical wind shears have been considered to be weak, the present simulation showed that vertical wind shears can intensify in winter. The enhanced migrating semi-diurnal tides, i.e., SW2 tides, had the most significant effects on VIC intensification in 2009. A possible mechanism of the SW2 tidal amplification is ZMZW variations due to the major SSW event in January–February 2009. Combined with the SSW effects, tidal modulations by 6–8-day PWs can also affect EsL intensity variations in the WiEsL intensification event. These results provided valuable insights

into the relationship between wintertime EsL intensity and lower atmospheric variations such as SSW events. We emphasize that this is the first study to succeed in reproducing WiEsL intensification occurrences driven by SSW events and exhibit a connection between VIC and WiEsL intensification, which was not examined by the previous studies.

Abbreviations

DAfoEs	Daily average foEs
DOY	Day of year
EsL	Sporadic E layer
GAIA	Ground-to-topside model of Atmosphere and Ionosphere for Aeronomy
LT	Local time
PW	Planetary wave
SSW	Sudden stratospheric warming)
VIC	Vertical ion convergence
WiEsL	Wintertime sporadic E layer
ZMZW	Zonal mean zonal wind
3D	Three-dimensional

Acknowledgements
We acknowledge the GAIA project for providing the neutral wind dataset. This work was supported by the"Nagoya University High-Performance Computing Research Project for Joint Computational Science"and Grant-in-Aid for JSPS Fellows (JP21J13173).

Author contributions
SA developed the ionospheric numerical model for metal ion layers and conducted the simulations, and wrote the paper. AS supervised this study and contributed to revising the paper. HS prepared datasets used in this study and contributed to revising the paper.

Funding
Funding was provided by Grant-in-Aid for JSPS Fellows (JP21J13173).

Availability of data and materials
The Ap and F10.7 indices on each simulated day and year were obtained from the Data Analysis Center for Geomagnetism and Space Magnetism, Kyoto University (http://wdc.kugi.kyoto-u.ac.jp/kp/index.html) and NOAA/NCEI (https://www.ngdc.noaa.gov/stp/space-weather/solar-data/solar-features/solar-radio/noontime-flux/penticton/penticton_observed/tables/), respectively. Ionosonde data were provided by the National Institute of Information and Communications Technology in Japan (https://wdc.nict.go.jp/IONO/HP2009/ISDJ/index-E.html). Raw data of GAIA model are available at https://gaia-web.nict.go.jp/data_e.html. The simulation data are available from the corresponding author upon reasonable request.

Declarations

Competing interests
The authors declare that they have no competing interests.

Author details
[1]National Institute of Information and Communications Technology, Tokyo, Japan. [2]Graduate School of Science, Kyoto University, Kyoto, Japan. [3]International Research Center for Space and Planetary Environmental Science, Kyushu University, Fukuoka, Japan.

Received: 31 August 2023 Accepted: 15 January 2024
Published online: 23 April 2024

References

Andoh S, Saito A, Shinagawa H, Ejiri MK (2020) First simulations of day-to-day variability of mid-latitude sporadic E layer structures. Earth Planets Space. https://doi.org/10.1186/s40623-020-01299-8

Andoh S, Saito A, Shinagawa H (2021) Temporal evolution of three-dimensional structures of metal ion layer around Japan simulated by a midlatitude ionospheric model. J Geophys Res Space Physics 126(6):e2021JA029. https://doi.org/10.1029/2021JA029267

Andoh S, Saito A, Shinagawa H (2022) Numerical simulations on day-to-day variations of low-latitude Es layers at Arecibo. Geophys Res Lett 49:e2021GL097. https://doi.org/10.1029/2021GL097473

Arras C, Wickert J (2018) Estimation of ionospheric sporadic E intensities from GPS radio occultation measurements. J Atmospheric Solar-Terrestrial Phys 171:60–63. https://doi.org/10.1016/j.jastp.2017.08.006

Arras C, Wickert J, Beyerle G, Heise S, Schmidt T, Jacobi C (2008) A global climatology of ionospheric irregularities derived from GPS radio occultation. Geophys Res Lett. https://doi.org/10.1029/2008GL034158

Axford WI (1963) The formation and vertical movement of dense ionized layers in the ionosphere due to neutral wind shears. J Geophys Res 68(3):769–779. https://doi.org/10.1029/JZ068i003p00769

Bautista MA, Romano P, Pradhan AK (1998) Resonance-averaged photoionization cross sections for astrophysical models. Astrophys J Supplement Series 118:259–265. https://doi.org/10.1086/313132

Bones DL, Plane JMC, Feng W (2016) Dissociative recombination of FeO^+ with electrons: Implications for plasma layers in the ionosphere. J Phys Chem A 120:1369–1376

Butler AH, Sjoberg JP, Seidel DJ, Rosenlof KH (2017) A sudden stratospheric warming compendium. Earth Syst Sci Data 9(1):63–76. https://doi.org/10.5194/essd-9-63-2017

Carrillo-Sánchez JD, Plane JMC, Feng W, Nesvorný D, Janches D (2015) On the size and velocity distribution of cosmic dust particles entering the atmosphere. Geophys Res Lett 42(15):6518–6525. https://doi.org/10.1002/2015GL065149

Chandra H, Sharma S, Devasia CV, Subbarao KSV, Sridharan R, Sastri JH, Rao JVSV (2001) Sporadic-E associated with the Leonid meteor shower event of November 1998 over low and equatorial latitudes. Ann Geophys 19(1):59–69. https://doi.org/10.5194/angeo-19-59-2001

Chang LC, Palo SE, Liu HL (2011) Short-term variability in the migrating diurnal tide caused by interactions with the quasi 2 day wave. J Geophys Res Atmos. https://doi.org/10.1029/2010JD014996

Christakis N, Haldoupis C, Zhou Q, Meek C (2009) Seasonal variability and descent of mid-latitude sporadic E layers at Arecibo. Ann Geophys 27(3):923–931. https://doi.org/10.5194/angeo-27-923-2009

Chu X, Yu Z (2017) Formation mechanisms of neutral Fe layers in the thermosphere at Antarctica studied with a thermosphere-ionosphere Fe/Fe^+ (TIFe) model. J Geophys Res Space Phys 122(6):6812–6848. https://doi.org/10.1002/2016JA023773

Chu YH, Wang CY, Wu KH, Chen KT, Tzeng KJ, Su CL, Feng W, Plane JMC (2014) Morphology of sporadic E layer retrieved from COSMIC GPS radio occultation measurements: wind shear theory examination. J Geophys Res Space Phys 119(3):2117–2136. https://doi.org/10.1002/2013JA019437

England SL, Englert CR, Harding BJ, Triplett CC, Marr K, Harlander JM, Swenson GR, Maute A, Immel TJ (2022) Vertical shears of horizontal winds in the lower thermosphere observed by icon. Geophys Res Lett 49(11):e2022098. https://doi.org/10.1029/2022GL098337

Feng W, Marsh DR, Chipperfield MP, Janches D, Höffner J, Yi F, Plane JMC (2013) A global atmospheric model of meteoric iron. J Geophys Res Atmos 118(16):9456–9474. https://doi.org/10.1002/jgrd.50708

Finney JW, Smith EK (1960) Report on the IGY oblique-incidence sporadic-E and F-scatter program Chap. 3. US Department of Commerce. Office of Technical Services

Forbes JM (1995) Tidal and planetary waves The Upper Mesosphere and Lower Thermosphere. Rev Exp Theory. https://doi.org/10.1029/GM087p0067

Forbes JM (1996) Planetary waves in the thermosphere-ionosphere system. J Geomagn Geoelectr 48:91–98

Forbes JM, Maute A, Zhang X, Hagan ME (2018) Oscillation of the ionosphere at planetary-wave periods. J Geophys Res Space Phys 123(9):7634–7649. https://doi.org/10.1029/2018JA025720

Griffith MJ, Mitchell NJ (2022) Analysis of migrating and non-migrating tides of the Extended Unified Model in the mesosphere and lower thermosphere. Ann Geophys 40:327–358. https://doi.org/10.5194/angeo-40-327-2022

Haldoupis C (2011) A tutorial review on sporadic E layers. In: Abdu MA, Pancheva D (eds) Aeronomy of the Earth's Atmosphere and Ionosphere. Springer, Netherlands, pp 381–394.
Haldoupis C (2012) Midlatitude sporadic e. a typical paradigm of atmosphere-ionosphere coupling. Space Sci Rev 168:1–21. https://doi.org/10.1007/s11214-011-9786-8
Haldoupis C, Pancheva D (2002) Planetary waves and midlatitude sporadic e layers: Strong experimental evidence for a close relationship. J Geophys Res Space Phys 107(A6):SIA 3Ã¢â‚¬â€œ1-SIA 3Ã¢â‚¬â€œ6. https://doi.org/10.1029/2001JA000212
Haldoupis C, Pancheva D, Singer W, Meek C, MacDougall J (2007) An explanation for the seasonal dependence of midlatitude sporadic E layers. J Geophys Res Space Phys. https://doi.org/10.1029/2007JA012322
Helmer M, Plane JMC, Qian J, Gardner CS (1998) A model of meteoric iron in the upper atmosphere. J Geophys Res Atmos 10:10913–10925. https://doi.org/10.1029/97JD03075
Jacobi C, Arras C, Wickert J (2013) Enhanced sporadic E occurrence rates during the Geminid meteor showers 2006–2010. Adv Radio Sci 11:313–318. https://doi.org/10.5194/ars-11-313-2013
Jin H, Miyoshi Y, Fujiwara H, Shinagawa H, Terada K, Terada N, Ishii M, Otsuka Y, Saito A (2011) Vertical connection from the tropospheric activities to the ionospheric longitudinal structure simulated by a new Earth's whole atmosphere-ionosphere coupled model. J Geophys Res Space Phys. https://doi.org/10.1029/2010JA015925
Jin H, Miyoshi Y, Pancheva D, Mukhtarov P, Fujiwara H, Shinagawa H (2012) Response of migrating tides to the stratospheric sudden warming in 2009 and their effects on the ionosphere studied by a whole atmosphere-ionosphere model GAIA with COSMIC and TIMED/SABER observations. J Geophys Res Space Phys 117(10):A10323
Kopp E (1997) On the abundance of metal ions in the lower ionosphere. J Geophys Res Space Phys 102(A5):9667–9674. https://doi.org/10.1029/97JA00384
Koushik N, Kumar K, Pramitha M (2022) A tropical stratopause precursor for sudden stratospheric warmings. Sci Reports 12:2937. https://doi.org/10.1038/s41598-022-06864-7
Lindzen RS, Chapman S (1969) Atmospheric tides. Space Sci Rev 10:3–188. https://doi.org/10.1007/BF00171584
Liu HL (2017) Large wind shears and their implications for diffusion in regions with enhanced static stability: The mesopause and the tropopause. J Geophys Res Atmos 122(18):9579–9590. https://doi.org/10.1002/2017JD026748
Liu HL, Roble RG (2002) A study of a self-generated stratospheric sudden warming and its mesospheric-lower thermospheric impacts using the coupled time-gcm/ccm3. J Geophys Res Atmos 107(D23):151–1518. https://doi.org/10.1029/2001JD001533
Liu HL, Li T, She CY, Oberheide J, Wu Q, Hagan ME, Xu J, Roble RG, Mlynczak MG, Russell JM III (2007) Comparative study of short-term diurnal tidal variability. J Geophys Res Atmos. https://doi.org/10.1029/2007JD008542
Luo J, Liu H, Xu X (2021) Sporadic E morphology based on COSMIC radio occultation data and its relationship with wind shear theory. Earth Planets Space 73:212
Maruyama T, Kato H, Nakamura M (2003) Ionospheric effects of the Leonid meteor shower in November 2001 as observed by rapid run ionosondes. J Geophys Res Space Phys. https://doi.org/10.1029/2003JA009831
Meyer CK (1999) Gravity wave interactions with mesospheric planetary waves: A mechanism for penetration into the thermosphere-ionosphere system. J Geophys Res Space Phys 104(A12):28181–28196. https://doi.org/10.1029/1999JA900346
Miyoshi Y, Fujiwara H (2008) Gravity waves in the thermosphere simulated by a general circulation model. J Geophys Res Atmos. https://doi.org/10.1029/2007JD008874
Miyoshi Y, Pancheva D, Mukhtarov P, Jin H, Fujiwara H, Shinagawa H (2017) Excitation mechanism of non-migrating tides. J Atmos Solar-Terrestrial Phys 156:24–36. https://doi.org/10.1016/J.JASTP.2017.02.012
Nahar SN, Bautista MA, Pradhan AK (1997) Electron-ion recombination of neutral iron. Astrophys J 479:497–503
Pancheva D, Haldoupis C, Meek CE, Manson AH, Mitchell NJ (2003) Evidence of a role for modulated atmospheric tides in the dependence of sporadic e layers on planetary waves. J Geophys Res Space Phys. https://doi.org/10.1029/2002JA009788
Pancheva D, Mitchella N, Middletona H, Muller H (2003) Variability of the semidiurnal tide due to fluctuations in solar activity and total ozone. J Atmos Sol Terr Phys 65:1–19. https://doi.org/10.1016/S1364-6826(02)00084-6
Pedatella NM, Forbes JM (2010) Evidence for stratosphere sudden warming-ionosphere coupling due to vertically propagating tides. Geophys Res Lett. https://doi.org/10.1029/2010GL043560
Pedatella NM, Liu H (2013) The influence of atmospheric tide and planetary wave variability during sudden stratosphere warmings on the low latitude ionosphere. J Geophys Res Space Phys 118(8):5333–5347. https://doi.org/10.1002/jgra.50492
Pedatella NM, Liu HL, Hagan ME (2012) Day-to-day migrating and nonmigrating tidal variability due to the six-day planetary wave. J Geophys Res Space Phys. https://doi.org/10.1029/2012JA017581
Pedatella NM, Liu HL, Richmond AD, Maute A, Fang TW (2012) Simulations of solar and lunar tidal variability in the mesosphere and lower thermosphere during sudden stratosphere warmings and their influence on the low-latitude ionosphere. J Geophys Res Space Phys. https://doi.org/10.1029/2012JA017858
Pedatella NM, Liu HL, Sassi F, Lei J, Chau J, Zhang X (2014) Ionosphere variability during the 2009 SSW: influence of the lunar semidiurnal tide and mechanisms producing electron density variability. J Geophys Res Space Phys 119(5):3828–3843. https://doi.org/10.1002/2014JA019849
Picone JM, Hedin AE, Drob DP, Aikin AC (2002) NRLMSISE-00 empirical model of the atmosphere: statistical comparisons and scientific issues. J Geophys Res Space Phys 107(A12):1468
Plane JMC (2012) Cosmic dust in the earth's atmosphere. Chem Soc Rev 41:6507–6518. https://doi.org/10.1039/C2CS35132C
Plane JMC, Cox RM, Rollason RJ (1999) Metallic layers in the mesopause and lower thermosphere region. Adv Space Res 24(11):1559–1570
Plane JMC, Feng W, Dawkins ECM (2015) The Mesosphere and Metals: Chemistry and Changes. Chem Rev 115(10):4497–4541. https://doi.org/10.1021/cr500501m
Rapp M, Plane JMC, Strelnikov B, Stober G, Ernst S, Hedin J, Friedrich M, Hoppe UP (2012) In situ observations of meteor smoke particles (msp) during the geminids 2010: constraints on msp size, work function and composition. Ann Geophys 30(12):1661–1673. https://doi.org/10.5194/angeo-30-1661-2012
Rutherford JA, Mathis RF, Turner BR, Vroom DA (1972) Formation of calcium ions by charge transfer. J Chem Phys 57(8):3087–3090
Shalimov S, Haldoupis C (2002) A model of mid-latitude e-region plasma convergence inside a planetary wave cyclonic vortex. Ann Geophys 20(8):1193–1201. https://doi.org/10.5194/angeo-20-1193-2002
Sherman JP, She CY (2006) Seasonal variation of mesopause region wind shears, convective and dynamic instabilities above fort collins, co: A statistical study. J Atmos Solar-Terrestrial Phys 68(10):1061–1074. https://doi.org/10.1016/j.jastp.2006.01.011
Shinagawa H, Miyoshi Y, Jin H, Fujiwara H (2017) Global distribution of neutral wind shear associated with sporadic E layers derived from GAIA. J Geophys Res Space Phys 122(4):4450–4465
Shinagawa H, Tao C, Jin H, Miyoshi Y, Fujiwara H (2021) Numerical prediction of sporadic E layer occurrence using GAIA. Earth Planets Space. https://doi.org/10.1186/s40623-020-01330-y
Sinno K (1980) On the time delay of the appearance of sporadic E following meteor activity. J Atnwspheric Temstrial Phys 42:35–39
Smith EK (1957) Worldwide occurrence of sporadic E Chap. 3. US Department of Commerce, National Bureau of Standards
Sobhkhiz-Miandehi S, Yamazaki Y, Arras C, Miyoshi Y, Shinagawa H (2022) Comparison of the tidal signatures in sporadic E and vertical ion convergence rate, using FORMOSAT-3/COSMIC radio occultation observations and GAIA model. Earth Planets Space. https://doi.org/10.1186/s40623-022-01637-y
Tang Q, Zhou C, Liu Y, Chen G (2020) Response of sporadic e layer to sudden stratospheric warming events observed at low and middle latitudes. J Geophys Res Space Phys 125(2):e2019JA027. https://doi.org/10.1029/2019JA027283
...Thébault E, Finlay CC, Beggan CD, Alken P, Aubert J, Barrois O, Bertrand F, Bondar T, Boness A, Brocco L, Canet E, Chambodut A, Chulliat A, Coïsson P, Civet F, Du A, Fournier A, Fratter I, Gillet N, Hamilton B, Hamoudi M, Hulot G, Jager T, Korte M, Kuang W, Lalanne X, Langlais B, Léger JM, Lesur V, Lowes FJ, Macmillan S, Mandea M, Manoj C, Maus S, Olsen N, Petrov V, Ridley V, Rother M, Sabaka TJ, Saturnino D, Schachtschneider R, Sirol

O, Tangborn A, Thomson A, TØffner-Clausen L, Vigneron P, Wardinski I, Zvereva T, (2015) International geomagnetic reference field: the 12th generation. Earth Planets Space 67:79
Vondrak T, Woodcock KRI, Plane JMC (2006) A kinetic study of the reactions of Fe^+ with N_2O, N_2, O_2, CO_2 and H_2O, and the ligand-switching reactions $Fe^+ \cdot X + Y \rightarrow Fe^+ \cdot Y + X$ ($X = N_2, O_2, CO_2$; $Y = O_2, H_2O$). Phys Chem Chem Phys 8:503–512. https://doi.org/10.1039/B508922K
Whitehead JD (1961) The formation of the sporadic-E layer in the temperate zones. J Atmos Terrestrial Phys 20(1):49–58
Whitehead JD (1989) Recent work on mid-latitude and equatorial sporadic-E. J Atmos Terrestrial Phys 51(5):401–424
Woodcock KRS, Vondrak T, Meech SR, Plane JMC (2006) A kinetic study of the reactions $FeO^+ + O$, $Fe^+ \cdot N2 + O$, $Fe^+ \cdot O2 + O$ and $FeO^+ + CO$: Implications for sporadic E layers in the upper atmosphere. Phys Chem Chem Phys 8:1812–1821
Wu DL, Ao CO, Hajj GA, De La Torre Juarez M, Mannucci AJ (2005) Sporadic E morphology from GPS-CHAMP radio occultation. J Geophys Res Space Phys 110(A1):A01. https://doi.org/10.1029/2004JA010701
Wu J, Feng W, Liu HL, Xue X, Marsh DR, Plane JMC (2021) Self-consistent global transport of metallic ions with WACCM-X. Atmos Chem Phys 21(20):15619–15630. https://doi.org/10.5194/acp-21-15619-2021
Yamazaki Y (2018) Quasi-6-day wave effects on the equatorial ionization anomaly over a solar cycle. J Geophys Res Space Phys 123(11):9881–9892. https://doi.org/10.1029/2018JA026014
Yamazaki Y, Arras C, Andoh S, Miyoshi Y, Shinagawa H, Harding BJ, Englert CR, Immel TJ, Sobhkhiz-Miandehi S, Stolle C (2022) Examining the wind shear theory of sporadic E With ICON/MIGHTI winds and COSMIC-2 radio occultation data. Geophys Res Lett 49(1):e2021096. https://doi.org/10.1029/2021GL096202
Yeh WH, Liu JY, Huang CY, Chen SP (2014) Explanation of the sporadic-E layer formation by comparing FORMOSAT-3/COSMIC data with meteor and wind shear information. J Geophys Res Atmos 119(8):4568–4579. https://doi.org/10.1002/2013JD020798
Yiğit E, Medvedev AS (2017) Influence of parameterized small-scale gravity waves on the migrating diurnal tide in earth's thermosphere. J Geophys Res Space Phys 122(4):4846–4864. https://doi.org/10.1002/2017JA024089
Yu B, Xue X, Yue X, Yang C, Yu C, Dou X, Ning B, Hu L (2019) The global climatology of the intensity of the ionospheric sporadic E layer. Atmos Chem Phys 19(6):4139–4151. https://doi.org/10.5194/acp-19-4139-2019
Yu B, Xue X, Scott CJ, Wu J, Yue X, Feng W, Chi Y, Marsh DR, Liu H, Dou X, Plane JMC (2021) Interhemispheric transport of metallic ions within ionospheric sporadic *e* layers by the lower thermospheric meridional circulation. Atmos Chem Phys 21(5):4219–4230. https://doi.org/10.5194/acp-21-4219-2021
Zuo X, Wan W (2008) Planetary wave oscillations in sporadic E layer occurrence at Wuhan. Earth Planet Space 60:647–652. https://doi.org/10.1186/BF03353128

Publisher's Note